NANO LETTERS

2006
Vol. 6, No. 4
725−729

Fabrication and Characterization of Three-Dimensional InGaAs/GaAs Nanosprings

Dominik J. Bell, Lixin Dong, and Bradley J. Nelson*

Institute of Robotics and Intelligent Systems, ETH Zurich, 8092 Zurich, Switzerland

Matthias Golling

FIRST Centre for Micro- and Nanoscience, ETH Zurich, 8093 Zurich, Switzerland

Li Zhang and Detlev Grützmacher

Laboratory for Micro- and Nanotechnology, Paul Scherrer Institute, 5232 Villigen, Switzerland

Received December 21, 2005; Revised Manuscript Received February 15, 2006

ABSTRACT

This paper presents the use of a novel fabrication technique to produce three-dimensional (3D) nanostructures. The process is based on conventional microfabrication techniques to create a planar pattern in an InGaAs/GaAs bilayer that self-assembles into 3D structures during a wet etch release. The nanostructures are proposed to function as nanosprings for electromechanical sensors. Nanomanipulation inside a scanning electron microscope (SEM) was conducted to probe the structures for mechanical characterization. The results were validated by simulation.

Many three-dimensional (3D) helical structures with micro- and nanofeatures have been synthesized from different materials. Typical examples include carbon microcoils based on amorphous carbon,[1] carbon nanocoils based on carbon nanotubes,[2] and zinc oxide nanobelts.[3,4] Because of their interesting morphology, as well as mechanical,[5] electrical,[6] and electromagnetic properties, these nanostructures can be used as components for micro and nanoelectromechanical systems (MEMS and NEMS) such as springs, magnetic field detectors, chemical or biological sensors, electromagnets, inductors, actuators, and high-performance electromagnetic wave absorbers.

A new method of creating structures with nanometer-scale dimensions has been presented recently.[7] The structures are created through a top-down fabrication process in which a strained nanometer-thick heteroepitaxial bilayer curls up to form 3D structures with nanoscale features. Several techniques have been proposed to improve the control over the fabrication process in terms of the resulting length, shape, and orientation of structures based on III−V compounds.[8−11] In this paper, InGaAs/GaAs nanosprings were fabricated with one or two ends fixed to nonscrolling supports for control over their position. The anisotropy in stiffness of the bilayer was used to control their geometry and orientation after the release.

Recently, 3D nanosprings have been proposed to be used for electromechanical sensors.[12] For this purpose SiGe/Si/Cr and SiGe/Si nanosprings were characterized through experiments and simulation. In this paper the fabrication and characterization of InGaAs/GaAs nanosprings is presented. This material system is promising for use in electromechanical sensors, such as force or pressure sensors, particularly because these materials exhibit both piezoresistive and piezoelectric effects.[13,14] The flexible nanostructures serve as a mechanism to transduce force to displacement. Deformations are detected visually through piezoresistance or through piezoelectricity. All of these sensing mechanisms have been demonstrated previously with other structures on the micrometer scale. For example, the deformation of polysilicon beams has been detected visually to measure forces generated by living cells,[15] piezoresistive microcantilevers have been used to characterize low-force electrical contacts,[16] and piezoelectric sensors were employed in cantilevers for scanning probe microscopy.[17]

Characterization and fabrication of nanosensors have proven challenging problems. Previously, the mechanical response of carbon nanosprings was characterized with an atomic force microscope (AFM).[18] In this paper, nanoma-

* Corresponding author. E-mail: bnelson@ethz.ch.

10.1021/nl0525148 CCC: $33.50
Published on Web 03/11/2006

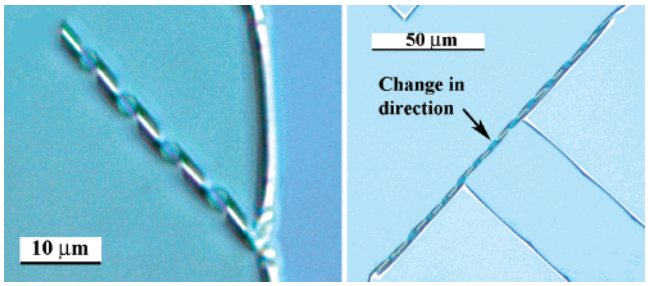

Figure 1. Digital microscope images of helical structures (a) fixed on one side (b) fixed on both sides. There is a change in winding direction in the center.

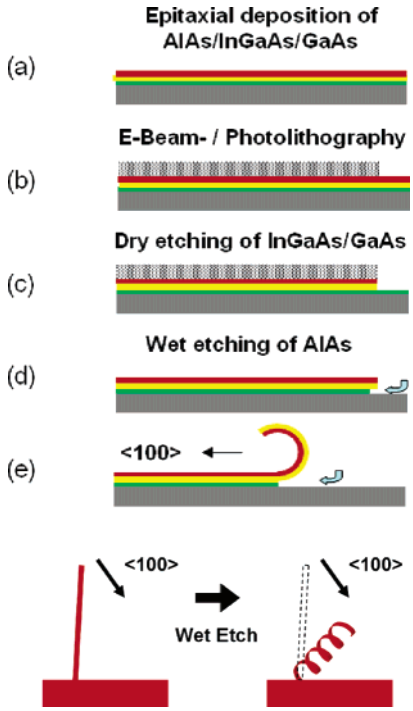

Figure 2. Basic process sequence and schematic top view: initial planar bilayer, patterned through conventional microfabrication techniques assembles itself into 3D nanostructures during wet etch release.

nipulation[19] inside an SEM is applied for characterizing mechanical properties of the nanostructures.

Figure 1 shows SEM images of typical helical nanostructures taken with a digital microscope (Leica, DM4000 M). The structures are made of an InGaAs/GaAs bilayer. In Figure 1a the nanospring is fixed on one side after fabrication. In Figure 1b it is fixed on both sides, and the two halves of the nanospring have opposite winding directions.

Figure 2 illustrates the fabrication process. The initial layers were grown on semi-insulating GaAs (Freiberger Compound Materials) using a molecular beam epitaxy system (VEECO, Gen III MBE) equipped with a valved cracker for As and solid sources for Ga and In. For n-type doping, a solid Si source was used. Substrate temperature was determined by diffuse reflectance spectroscopy. Standard growth conditions were applied with a V/III ratio around 40 and growth rates of approximately 0.1 nm/s. A sacrificial layer of AlAs was grown onto a GaAs buffer layer at 580 °C. The subsequent 11-nm-thick InGaAs layer was deposited at

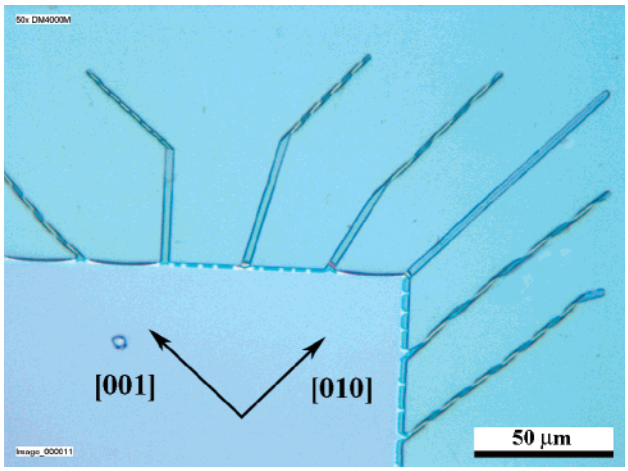

Figure 3. Digital microscope image with released helical structures. The different orientations of the initial pattern result in helical structures with different pitches.

510 °C. An In content of 14% was determined by X-ray diffraction measurements. The thickness of this layer must be smaller than the critical thickness to maintain elastic strain.[20,21] Finally, a 16-nm-thick GaAs layer, n-type doped to 5×10^{17} cm^{-3}, was deposited (Figure 2a). The initial pattern can be created through photolithography (Figure 2b). S1805 was used as a resist. After the development of the resist with MF319, RIE with a mixture of 95 sccm H_2 and 5 sccm CH_4 gases at a pressure of 130 μbar, a substrate temperature of 10 °C, and a power of 130 W was used to transfer the pattern to the InGaAs/GaAs bilayers at an etch rate of approximately 3.33 nm/s (Figure 2c). After the remaining photoresist was removed, a 1% HF aqueous solution was used to selectively etch the AlAs sacrificial layer under the InGaAs/GaAs heterostructures for the self-assembly of the nanostructures (Figure 2d). During this wet etch, the patterned bilayer curled up along a ⟨100⟩ direction releasing the internal strain and forming 3D structures (Figure 2e). The direction of the scrolling is determined by the anisotropy in stiffness of the InGaAs/GaAs bilayer. After the wet etch release, the samples were rinsed in deionized water and subsequently in isopropyl alcohol. Finally, they were dried with a supercritical CO_2 dryer so that the structures would not be damaged from surface tension. After exposure to air at room temperature, a thin native oxide layer forms on the surfaces of the released nanostructures.[22]

A helical geometry can be achieved through this process if a rectangular shape is used as the initial planar pattern with an orientation at some angle relative to the ⟨100⟩ directions, as illustrated in Figure 2. The structures roll up such that they align themselves with the closest ⟨100⟩ direction. For a stripe that is aligned with a ⟨110⟩ direction there are two possible rolling directions. The angle between the patterned stripe and the closest ⟨100⟩ direction determines the pitch between turns of the resulting helical structures. This is illustrated by the images in Figure 3. The initial 2D pattern was made of stripes with the angle of orientation decreasing in steps of 15°. The initial pattern is still visible for some of the structures that are not fully released, as well

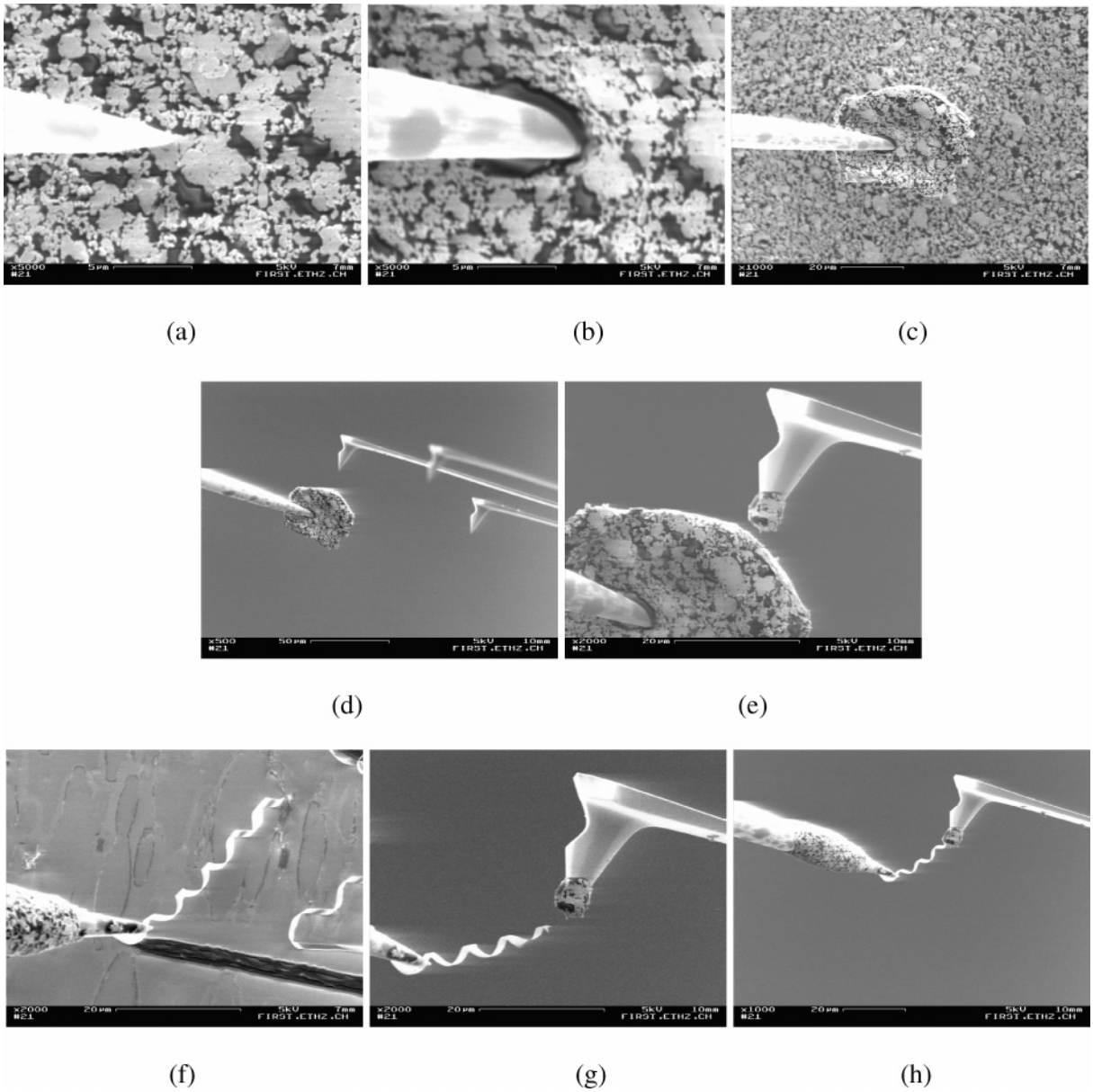

Figure 4. SEM images of the experimental procedure. (a−c) Dip probe in droplet of conductive epoxy on the chip. (d−e) Dip AFM tip in droplet attached to probe tip. (f−h) Break and pick up nanospring and attach it to AFM tip.

as for the stripe with an orientation parallel to the [010] direction.

For the mechanical characterization experiments, a nanomanipulator (Kleindiek, MM3A) and an AFM cantilever (Mikromasch, CSC38/Ti−Pt, nominal stiffness 0.03 N/m) were installed inside an SEM (Zeiss, DSM 962). The AFM cantilever was calibrated using the Sader method,[23] and the stiffness was found to be 0.08 N/m. The experimental procedure is illustrated in Figure 4. A metal probe (Picoprobe, T-4-10-1mm) with a tip radius of 100 nm, mounted on the nanomanipulator was first dipped into a conductive epoxy (Transene, Nanopoxy) in order to coat the probe with glue (Figure 4a−c). Then, the AFM tip was dipped into the glue attached on the probe in order to cover the tip of the AFM cantilever with glue as well (Figure 4d and e). Next, the probe was used to break and pick up a nanospring on one side and attach it to the AFM tip on the other side (Figure 4f−h).

After a nanospring was attached as described above, a tensile force was applied to it by moving the probe away from the AFM cantilever in the axial direction of the nanospring. Continuous frames of images were taken to detect the deflection of the cantilever and the relative displacement of the probe from the AFM cantilever. When the tensile force was increased further after the last measurement point, the attachment between the nanospring and the AFM cantilever broke, and the nanosprings returned to their initial shape at the zero-displacement position. This indicates that there was no plastic deformation. The characterization was carried out for three different nanosprings. Their dimensions are summarized in Table 1. The nanosprings were fabricated on different chips of the same wafer. The difference in diameters indicates some inhomogeneity of the MBE deposition. For the number of turns, only those turns that were unconstrained between the probe and the AFM

Table 1. Specifications of Nanosprings Used in Experiments and Simulations

nanospring	1	2	3
thickness $In_{0.14}Ga_{0.86}$ As	11 nm		
thickness GaAs	16 nm		
diameter	2.02 μm	2.62 μm	2.59 μm
pitch	4.71 μm	6.17 μm	7.40 μm
width of wire in axial direction	3.14 μm	1.93 μm	3.82 μm
number of turns	9	3	2

tip were counted. It was checked from the images that the boundary conditions did not change during the experiments.

The SEM images were analyzed to extract the AFM tip displacement and the nanospring deformation, that is, the relative displacement of the probe from the AFM tip. From this displacement data and the known stiffness of the AFM cantilever, the tensile force acting on the nanosprings versus the nanospring displacement was plotted. The results are shown in Figure 5a for all three nansprings summarized in Table 1. The error bars represent the uncertainty in the deflection of the AFM cantilever and the nanospring given by the resolution of the SEM (1 μm at 3000x magnification), as well as the uncertainty in the calibration result of the AFM cantilever with the Sader method[23] that was estimated elsewhere.[24] In Figure 5b the stiffness is plotted versus the displacement. The elongation of the nanosprings in percent of their initial length is plotted in Figure 5c. From Figure 5a and b, it can be seen that the nanosprings exhibit low stiffness. The initial stiffness of nanospring 1 is as low as 0.0178 N/m. Therefore, they are suitable for high-resolution force sensors. Moreover, the overall elastic elongation capability is high, guaranteeing a large range of operation. For nanospring 1, an overall elastic strain of 48% was measured when the attachment to the AFM tip broke. Even after this large deflection the nanospring returned to its original shape at zero displacement, indicating that there was no plastic deformation. The elastic limit could not be reached in the force-displacement measurements because the attachments on both ends of the nanosprings did not withstand high enough forces. In a separate experiment, a nanospring was also exited at its resonance frequency both in bending mode and in the axial displacement mode. Because the resonance frequency did not change during 10^6 cycles it can be assumed that the mechanical properties of the bilayer material do not change with multiple loading. The plots in Figure 5a and b indicate that for sensors operating at lower values of nanospring elongation the relation between force and displacement is close to linear.

Finite element simulation was used to validate the experimental data. Only linear small-displacement simulation was carried out. This seemed sufficient for the purpose of validating the experimental results. The dimensions of the nanosprings used in the simulation were the same as those in the experiments, as summarized in Table 1. They were modeled consisting of two different layers, similar to the actual nanosprings. Values of the material properties in the model were taken from ref 25 with the rule of mixture applied for the InGaAs layer. Boundary conditions were

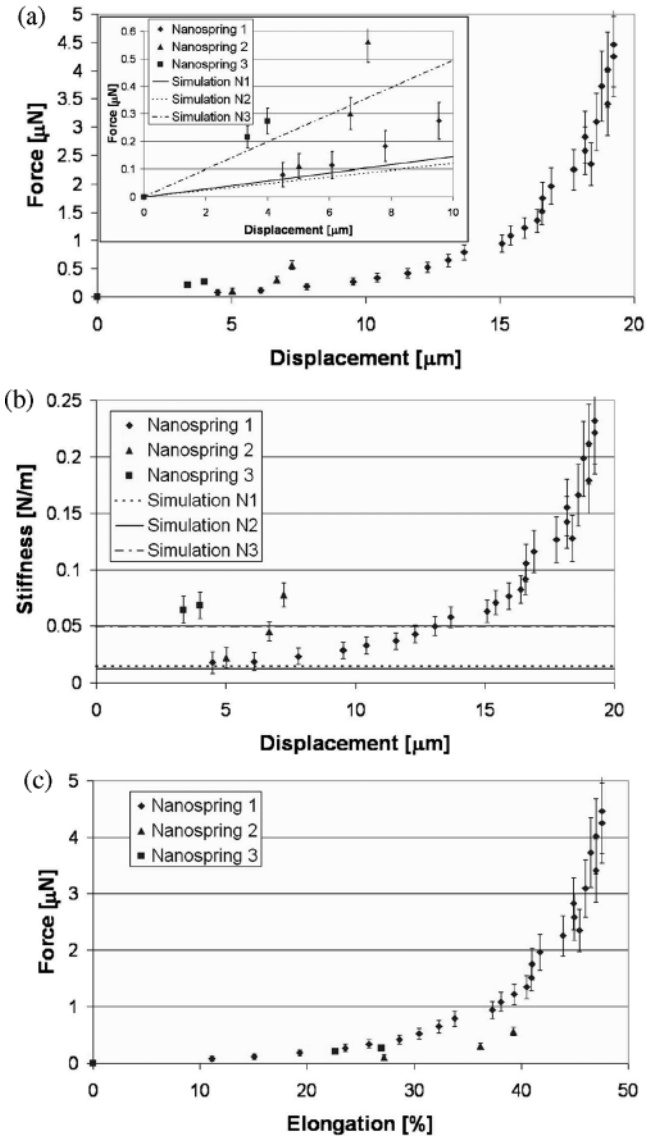

Figure 5. Experimental results and results from linear small-displacement simulation for three nanosprings. (a) Axial force vs displacement. (b) Stiffness vs displacement. (c) Axial force vs elongation.

applied to both ends of the nanosprings. On both ends they were constrained from rotation around all three axes. Moreover, on one end they were constrained from all translational movements, and on the other end they were constrained from translational movement perpendicular to the axial direction. On this end, a force in the axial direction was applied so that the displacement of this end in the axial direction could be computed. In Figure 6a, a plot of the displacement along the axial direction is shown for nanospring 1 from Table 1 with an applied axial force of 0.1 μN. In Figure 6b, an SEM image illustrates the corresponding experiment. The results from small-displacement simulations for all nanosprings are illustrated in the plots of Figure 5 as straight lines. With the satisfactory agreement between experiment and simulation, the simulation can be used to design nanosprings with a specified stiffness.

From the fabrication and characterization results, the helical nanostructures also appear to be suitable to function

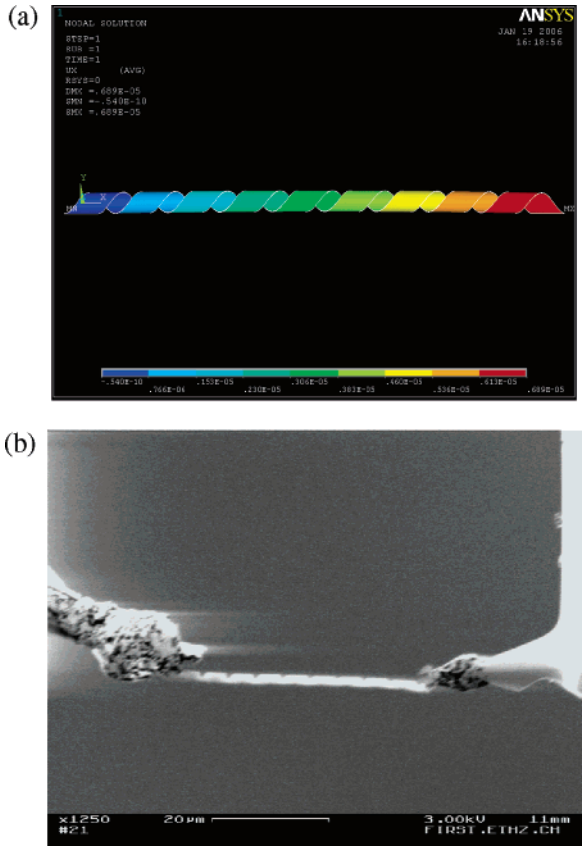

Figure 6. (a) Structural simulation for nanospring with nine turns: axial displacement in meters for an axial tensile force of 0.1 μN on one end and fixed on the other end. (b) SEM image of the corresponding experiment.

as inductors. They allow further miniaturization compared to state-of-the-art microinductors. For this purpose, higher doping of the bilayer and an additional metal layer would result in improved conductance, inductance, and quality factor. Moreover, a semiconductive helical structure, when functionalized with binding molecules, can be used for chemical sensing under the same principle as demonstrated with other types of nanostructures.[26] The electrical properties of the 3D structure can be controlled well during the deposition of the bilayer for this purpose. Moreover, with bilayers in the range of a few monolayers, the resulting structures would exhibit very high surface-to-volume ratios with the whole surface exposed to an incoming analyte. Therefore, high sensitivity could be achieved.

Nanospring structures were fabricated using a self-assembled fabrication process. Nanomanipulation in SEM was used for their mechanical characterization. A satisfactory agreement was obtained between the mechanical characterization of the 3D nanostructures and predictions from simulations. With their low-stiffness and high-strain capability the nanosprings can be used as high-resolution and large-range force sensors in conjunction with visual displacement measurement. Moreover, the piezoresistive and piezoelectric behavior of doped InGaAs/GaAs nanosprings can be used for electromechanical sensors. By varying design parameters, such as the number of turns, thickness, diameter, or pitch, a nanospring with the required stiffness can be designed through simulation. Nanomanipulation in SEM was demonstrated as a powerful experimental technique with potential for the assembly of NEMS. The fabrication process is suitable for further miniaturization. Nanometer-scale diameter and wire width can be achieved through changes in the layer design and electron beam lithography, respectively.

Supporting Information Available: Resonance experiments. This material is available free of charge via the Internet at http://pubs.acs.org.

References

(1) Motojima, S.; Kawaguchi, M.; Nozaki, K.; Iwanaga, H. *Appl. Phys. Lett.* **1990**, *56*, 321−323.
(2) Zhang, X. B.; Zhang, X. F.; Bernaerts, D.; Vantendeloo, G. T.; Amelinckx, S.; Vanlanduyt, J.; Ivanov, V.; Nagy, J. B.; Lambin, P.; Lucas, A. A. *Europhys. Lett.* **1994**, *27*, 141−146.
(3) Gao, P. M.; Ding, Y.; Mai, W. J.; Hughes, W. L.; Lao, C. S.; Wang, Z. L. *Science* **2005**, *309*, 1700−1704.
(4) Kong, X. Y.; Wang, Z. L. *Nano Lett.* **2003**, *3*, 1625−1631.
(5) Chen, X. Q.; Zhang, S. L.; Dikin, D. A.; Ding, W. Q.; Ruoff, R. S.; Pan, L. J.; Nakayama, Y. *Nano Lett.* **2003**, *3*, 1299−1304.
(6) Kaneto, K.; Tsuruta, M.; Motojima, S. *Synth. Met.* **1999**, *103*, 2578−2579.
(7) Prinz, V. Y.; Seleznev, V. A.; Gutakovsky, A. K.; Chekhovsky, A. V.; Preobrazhenskii, V. V.; Putyato, M. A.; Gavrilova, T. A. *Physica E* **2000**, *6*, 828−831.
(8) Prinz, A. V.; Prinz, V. Y.; Seleznev, V. A. *Microelectron. Eng.* **2003**, *67*−*8*, 782−788.
(9) Schmidt, O. G.; Deneke, C.; Schmarje, N.; Müller, C.; Jin-Phillipp, N. Y. *Mater. Sci. Eng., C* **2002**, *19*, 393−396.
(10) Prinz, V. Y.; Chekhovsky, A. V.; Preobrazhenskii, V. V.; Semyagin, B. R.; Gutakovsky, A. K. *Nanotechnology* **2002**, *13*, 231−233.
(11) Vorobèv, A. B.; Prinz, V. Y. *Semicond. Sci. Technol.* **2002**, *17*, 614−616.
(12) Bell, D. J.; Sun, Y.; Zhang, L.; Dong, L. X.; Nelson, B. J.; Grützmacher, D. *Sens. Actuators, A,* in press, 2006.
(13) Hsu, Y. W.; Lu, S. S.; Chang, P. Z. *J. Appl. Phys.* **1999**, *85*, 333−340.
(14) Hjort, K.; Soderkvist, J.; Schweitz, J. A. *J. Micromech. Microeng.* **1994**, *4*, 1−13.
(15) Lin, G.; Pister, K. S. J.; Roos, K. P. *J. Microelectromech. Syst.* **2000**, *9*, 9−17.
(16) Pruitt, B. L.; Park, W. T.; Kenny, T. W. *J. Microelectromech. Syst.* **2004**, *13*, 220−229.
(17) Kim, Y. S.; Lee, C. S.; Jin, W. H.; Jang, S.; Nam, H. J.; Bu, J. U. *Sens. Mater.* **2005**, *17*, 57−63.
(18) Poggi, M. A.; Boyles, J. S.; Bottomley, L. A. *Nano Lett.* **2004**, *4*, 1009−1016.
(19) Fukuda, T.; Arai, F.; Dong, L. X. *Proc. IEEE* **2003**, *91*, 1803−1818.
(20) Sasaki, A. *J. Cryst. Growth* **1996**, *160*, 27−35.
(21) Tanner, B. K.; Parbrook, P. J.; Whitehouse, C. R.; Keir, A. M.; Johnson, A. D.; Jones, J.; Wallis, D.; Smith, L. M.; Lunn, B.; Hogg, J. H. C. *Appl. Phys. Lett.* **2000**, *77*, 2156−2158.
(22) Torkhov, N. A. *Semiconductors* **2003**, *37*, 1177−1184.
(23) Sader, J. E.; Chon, J. W. M.; Mulvaney, P. *Rev. Sci. Instrum.* **1999**, *70*, 3967−3969.
(24) Clifford, C. A.; Seah, M. P. *Nanotechnology* **2005**, *16*, 1666−1680.
(25) Nakajima, K. *Jpn. J. Appl. Phys., Part 1* **1999**, *38*, 1875−1883.
(26) Cui, Y.; Wei, Q. Q.; Park, H. K.; Lieber, C. M. *Science* **2001**, *293*, 1289−1292.

NL0525148